This is a repository copy of *II. Analysis of 3D plasma motions in a chromospheric jet formed due to magnetic reconnection*.

White Rose Research Online URL for this paper:
http://eprints.whiterose.ac.uk/133582/

Version: Submitted Version

Article:

eprints@whiterose.ac.uk
https://eprints.whiterose.ac.uk/

II. ANALYSIS OF 3D PLASMA MOTIONS IN A CHROMOSPHERIC JET FORMED DUE TO MAGNETIC RECONNECTION

J.J. GONZÁLEZ-AVILÉS [1,2] , F.S. GUZMÁN [2], V. FEDUN [3], G. VERTH [4], R. SHARMA [4], S. SHELYAG [5] AND S. REGNIER [5]

[1] Instituto de Geofísica, Unidad Michoacán, Universidad Nacional Autónoma de México, Morelia, Michoacán, México.
[2] Laboratorio de Inteligencia Artificial y Supercómputo. Instituto de Física y Matemáticas, Universidad Michoacana de San Nicolás de Hidalgo. Morelia, Michoacán, México.
[3] Department of Automatic Control and Systems Engineering, University of Sheffield, Sheffield, S1 3JD, UK
[4] School of Mathematics and Statistics, University of Sheffield, Sheffield, S3 7RH, UK
[5] Department of Mathematics, Physics and Electrical Engineering, Northumbria University, Newcastle upon Tyne, NE1 8ST, UK
Draft version July 12, 2018

ABSTRACT

Within the framework of resistive MHD, implementing the C7 equilibrium atmosphere model and a 3D potential magnetic field realistic configuration, we simulate the formation of a plasma jet with the morphology, upward velocity up to 130 km/s and timescale formation between 60 and 90 s after beginning of simulation, similar to those expected for Type II spicules. Initial results of this simulation were published in Paper I e.g. González-Avilés et al. (2018) and present paper is devoted to the analysis of transverse displacements and rotational type motion of the jet. Our results suggest that 3D magnetic reconnection may be responsible for the formation of the jet in Paper I. In this paper, by calculating times series of the velocity components v_x and v_y in different points near to the jet for various heights we find transverse oscillations in agreement with spicule observations. We also obtain a time-distance plot of the temperature in a cross-cut at the plane $x =0.1$ Mm and find significant transverse displacements of the jet. By analyzing temperature isosurfaces of 10^4 K with the distribution of v_x, we find that if the line-of-sight (LOS) is approximately perpendicular to the jet axis then there is both motion towards and away from the observer across the width of the jet. This red-blue shift pattern of the jet is caused by rotational motion, initially clockwise and anti-clockwise afterwards, which could be interpreted as torsional motion. From a nearly vertical perspective of the jet the LOS velocity component shows a central blue-shift region surrounded by red-shifted plasma.

Keywords: magnetohydrodynamics (MHD) – methods: numerical – Sun: atmosphere

1. INTRODUCTION

In the solar atmosphere, jet-like structures, defined as an impulsive evolution of collimated bright or dark structure are observed in a wide range of environments. In particular, the upper chromosphere is full with spicules, thin jets of chromospheric plasma that reach heights of 10,000 km or move above the photosphere. Although spicules were described since 1878 by Secchi (Secchi 1878), understanding their physical nature has been a whole area of research (Beckers et al. 1968; Sterling 2000). There are two types of spicules, the first type of spicules are so-called Type I, which reach maximum heights of 4-8 Mm, maximum ascending velocities of 15-40 km s^{-1}, have a lifetime of 3-6.5 minutes (Pereira et al. 2012), and show up and downward motions (Beckers et al. 1968; Suematsu et al. 1995). These Type I spicules are probably the counterpart of the dynamic fibrils. They follow a parabolic (ballistic) path in space and time. In general the dynamics of these spicules is produced by mangneto-acoustic shock waves passing or wave-driving through the chromosphere (Shibata et al. 1982; De Pontieu et al. 2004; Hansteen et al. 2006; Martínez-Sykora et al. 2009; Matsumoto & Shibata 2010; Scullion et al. 2011). The second type of spicules are called Type II, which reach maximum heights of 3-9 Mm (longer in coronal holes) and have lifetimes of 50-150 s, shorter than that of Type I spicules (De Pontieu et al. 2007a; Pereira et al. 2012). These Type II spicules show apparent upward motion with speeds of order 30-110 km s^{-1}. At the end of their life they usually exhibit rapid fading in chromospheric lines (De Pontieu et al. 2007b). It has been suggested from observations that Type II spicules are continuously accelerated

while being heated to at least transition region temperatures (De Pontieu et al. 2009, 2011). Other observations indicate that some Type II spicules also show an increase or a more complex velocity dependence with height (Sekse et al. 2012).

Also, Type II spicules show other motions in addition to radial outflow. In the Ca II H line they are seen to sway transversely with amplitudes of order 10-20 km s^{-1} and periods of 100-500 s (De Pontieu et al. 2007b; Tomczyk et al. 2007; Zaqarashvili & Erdélyi 2009; McIntosh et al. 2011; Sharma et al. 2017), suggesting generation of upward, downward and standing Alfvén waves (Okamoto & De Pontieu 2011; Tavabi et al. 2015), the generation of MHD kink mode waves or Alfvén waves due to magnetic reconnection (Nishizuka et al. 2008; He et al. 2009; McLaughlin et al. 2012; Kuridze et al. 2012) or due to magnetic tension and ambipolar diffusion (Martínez-Sykora et al. 2017). For instance, Suematsu et al. (2008) suggest that some spicules show multi-thread structure as result of possible rotation. Another possible motion of Type II spicules is the torsional one as suggested by Beckers (1972) and Kayshap et al. (2018), and established using high-resolution spectroscopy at the limb (De Pontieu et al. 2012). According to the latter, Type II spicules show torsional motions rotational speeds of 25-30 km s^{-1}. In addition, the continuation of this kind of motion in the transition region and coronal lines suggest that they may help driving the solar wind (McIntosh et al. 2011).

There are other types of motion less well established, for instance Curdt & Tian (2011) and Curdt et al. (2012) suggest that the spinning motion of Type II spicules can explain the tilts of ultraviolet lines in the so-called explosive events producing larger-scale macro spicules. These spectral-line tilts
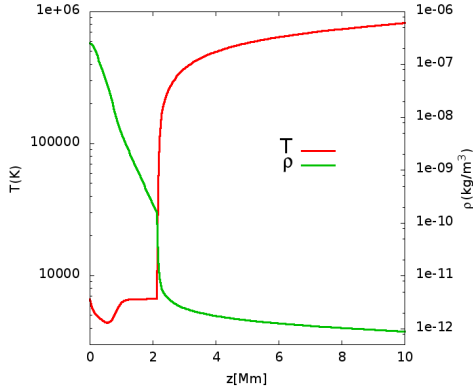
Figure 1. Temperature and mass density as a function of height z for the C7 equilibrium solar atmosphere model.

were observed at the limb and also attributed to spicule rotation (Beckers 1972). At smaller scales, evidence of rotating motions has been deduced for the chromospheric/transition region jet events (Liu et al. 2009, 2011). In addition, Tian et al. (2014) using the IRIS instrument found transverse motions as well as line broadening attributed to the existence of twist and torsional Alfvén waves. At the photospheric level, there is evidence that a fraction of spicules present twisting motions (Sterling et al. 2010a,b; De Pontieu et al. 2012). Beyond the resolution of imaging instruments, the spectrum of explosive events can also be interpreted as arising from the fast rotation of magnetic structures (Curdt & Tian 2011; Curdt et al. 2012). Apart from the small scale jets, Doppler images have shown that several coronal jet events present strong rotational motion, diagnosed with blue-red shift observed on opposite sides of each jet (Dere et al. 1989; Pike & Mason 1998; Cheung et al. 2015).

In this paper, we show that the jet with characteristics of a Type II spicule, obtained in the numerical simulations presented in González-Avilés et al. (2018) shows transverse displacements and rotational type motion initially clockwise and anti-clockwise afterwards.

The summary of the model and numerical methods are described in Section 2. The results of the numerical simulations are presented in Section 3. In Section 4, we present our final comments and conclusions.

2. SUMMARY OF THE MODEL AND NUMERICAL METHODS

The details of the numerical methods can be found in González-Avilés et al. (2018) and a brief summary is the following. We solve the resistive 3D MHD equations including the constant gravity field at the Sun's surface. We integrate the Extended Generalized Lagrange Multiplier (EGLM) resistive MHD (Jiang et al. 2012) using High Resolution Shock Capturing methods with an adaptive choice of Flux formula between HLLC and HLLE, combined with MINMOD and MC limiters.

For the initial magnetic field, we use a 3D potential (current-free) configuration extrapolated from a simulated quiet-Sun photospheric field, obtained from a large-scale, high-resolution, self-consistent simulation of solar magnetoconvection in a bipolar photospheric region with the MURaM code (Vögler et al. 2005; Shelyag et al. 2012). The computational box has a size of 480×480×400 pixels, with a spatial resolution of 25 km in the horizontal directions and 10 km in the vertical direction.

In order to model the atmosphere we choose the numerical domain to cover part of the interconnected solar photosphere, chromosphere and corona (see Figure 1). For this the atmosphere is initially assumed to be in hydrostatic equilibrium. The temperature field is considered to obey the semi-empirical C7 model of the chromosphere-transition region (Avrett & Loeser 2008) and is distributed consistently with observed line intensities and profiles from the SUMER atlas of the extreme ultraviolet spectrum (Curdt et al. 1999). The photosphere is extended to the solar corona as described by Fontela et al. (1990) and Griffiths et al. (1999). The temperature $T(z)$ and mass density $\rho(z)$ are functions of height z and are shown in Figure 1, where the transition region shows its characteristic steep gradient.

Once we set the initial magnetic field and the atmospheric model equilibria, the plasma evolves due to the inclusion of resistivity according to the EGLM equations. The evolution is tracked in a 3D numerical box with unigrid discretization of size $x \in [0,6]$, $y \in [0,6]$, $z \in [0,10]$ Mm, covered with $240 \times 240 \times 400$ grid cells, i.e., the effective resolution is 25 km in each direction. In the next section we focus on the transverse and rotational motions which appear during the evolution fo the jet.

3. RESULTS OF NUMERICAL SIMULATIONS

Transverse oscillations. A property to look into is the transverse displacement of the jet investigate if it is actually oscillating in a kink-like manner. We measure the velocity components v_x and v_y in time at three different points near and within the spicule, points A ($x = 1$, $y = 3$, z) Mm, points B ($x = 1$, $y = 3.5$, z) Mm and points C ($x = 1$, $y = 4$, z) Mm, for various values of z. Near these points the vector velocity field rotates as is illustrated at the top of Figure 2. We measure the value of the velocity components at heights $z = 2.5, 3.5, 5, 6.5$ and 8 Mm. The results displayed in Figure 2 tell us about the motion along the x and y directions. For example the horizontal component of velocity v_x at the various heights in point A shows transverse displacements with high amplitudes at the top of jet and small at the bottom. We can also see a change of sign, which indicates a transverse oscillation of at least one period. The behavior of v_x at points B and C is similar to that at point A. In the case of the v_y component at point A, we can see strong motions at the top, in particular there is a clear change of sing between 0 and 100 s, then we can identify oscillatory behavior at all heights, which is also clear at points B and C. By comparing the behavior of v_x and v_y we can conclude that the jet shows rotational motion, i.e. velocity components are out of phase, which will be reinforced by the following analysis.

Aside from analyzing the transverse motion at individual points in space, we can also identify the bulk transverse displacement of the jet in a horizontal cross-cut across the jet shown in a logarithm of temperature on the left of Figure 3. We measure this bulk transverse motion at a height of 7 Mm along a horizontal slice of length 3 Mm (blue line) centered at the mid-point of the domain in the y-direction (black line) as shown on the left of Figure 3. A time-distance plot of the logarithm of temperature along this slice as a function of time is shown on the right of Figure 3. From the time-distance plot we can see that from time $t = 50$ s the jet starts moving to the left until about time $t = 150$ s, jet starts moving to the right until it is displaced a horizontal distance of 3 Mm. This shows that simulated jet actually has a significant transverse motion during its lifetime. This phenomena is also observed

widely in spicule observations, see e.g., (De Pontieu et al. 2007b). To estimate the average speed of the transverse displacements, we indicate the center of the jet at the the times of maximum and minimum displacement up to 150 s with horizontal dashed blue lines on the right of Figure 3. The distance between the two lines is about 0.7 Mm (700 km) and the time between them is about 100 s, therefore the average speed is about 7 km s^{-1}.

Rotational motions. Another important property of Type II spicules to look at, is whether they are twisted, rotate or show an azimuthal flow component. Doppler shift observations of various emission lines in the limb suggest that Type II spicules are rotating (De Pontieu et al. 2012; Sekse et al. 2013; Sharma et al. 2017). From our simulation it is possible to study the behavior of the velocity components v_x and v_z inside the jet in order to track possible rotational or twisting motions. A similar analysis was carried out by Pariat et al. (2016) to identify torsional/twisting motions of coronal jets. In our case we show temperature contours with constant value of 10^4 K colored with the distribution of v_x at times $t = 30, 45, 60, 90, 105, 120, 150, 180$ and 210 s in Figure 4.

For the perspective used in this case, the blue color represents motion toward the reader and red color represents motion away from the observer. For instance, at time $t = 30$ s the jet starts to develop and shows both red and blue-shifted plasma. By times $t = 45$ and 60 s, the motions are predominantly towards the observer with counter-motion developing at the top of the jet. At time $t = 90$ s, the predominant motion towards the observer and some counter-motion still persists at the top of the jet. This dual behavior lasts through times $t = 105$ and $t = 120$ s. At times $t = 150, 180$ and 210 s the jet shows a velocity structure represented by a red-blue asymmetry across its width. The time evolution of the jet from the simulation (Figure 4) also shows strong resemblance to the observations of a spicule seen off-limb in Hα (Figure 5). Details of this observational data, e.g., time cadence and spatial resolution, have been discussed previously by Shetye et al. (2016). The unsharp mask intensity image (Figure 5(a)) of this spicule suggests it is launched from an inverted Y-shape structure (Shibata et al. 2007; He et al. 2009), associated with reconnection. The estimated Doppler shift profile (V_x), at discrete time-steps of the spicule evolution show striking similarities with the simulated jet. (Figure 5(b)) showcases the early rise-phase of the spicule ($t = 10$ s) as it starts to penetrate through the ambient chromospheric environment, as seen in Figure 4 ($t = 30$ s). At the middle-phase of it's evolution (Figure 4, $t = 105$ s), the spicule attains a mainly blue-shift Doppler profile, indicating bulk motion towards the observer as shown (Figure 5(c)). However, at the late-phase of the spicule's ascent, the apex has developed an asymmetric red-blue Doppler profile (Figure 5(d)), indicating rotational motion, similar to the simulated jet (Figure 4, t = 180 s). The rotational motion is prevalent at height above 3 Mm, as is also seen in the simulation.

These results together with the time series of the velocity components at points A, B, and C in Figure 2, clearly indicate rotational motions of the jet.

Vertical motion. In Figure 6 we show the isosurface of temperature colored with the values of v_z, which helps to track the vertical motion of the jet, for instance at times $t = 30, 45$ and 60 s, the jet practically shows upward motion from the middle to the top. By times $t = 90, 105$ and 120 s, the amplitude of vertical motion start to decrease at the bottom of the jet. Finally, at times $t = 150, 180$ and 210 s the jet starts moving downwards, in particular this behavior is consistent with the observed vertical motion with velocities of order 110 km s^{-1} in Type II spicules (Skogsrud et al. 2014).

4. CONCLUSIONS

In this paper by analyzing temperature isosurfaces to localize the jet, together with the analysis of the horizontal velocity components, we find that the development of a red-blue asymmetry across the jet is due to rotational motion. Interestingly, the rotational motion is initially clockwise and then begins to move in an anti-clockwise direction, indicating the presence of torsional motion. By analyzing the time series of v_x and v_y at points near and within the jet at different heights we showed that the rotational motion is generated in its upper region. In addition, by calculating a time-distance plot of the logarithm of temperature in a horizontal cross-cut at a height of 7 Mm it was shown that the jet also undergoes a considerable transverse displacement.

Additionally, we have presented observational support of rotational motion in an off-limb spicule appearing in the corona (and not being generated from below) in Figure 5(d). We can also see the simulated jet has a dual behavior (i) transverse motion at the foot (0-3 Mm) and (ii) twisted motion at the middle and top parts (3-10 Mm). The rotational type motion (initially clockwise and after anti-clockwise) can be interpreted as torsional starting at the top of the jet, when it reaches a region where the magnetic field dominates $\beta < 1$ as shown in Figure 7 and the Lorentz force is also bigger than pressure gradients $|\mathbf{J} \times \mathbf{B}| > |\nabla p|$ as shown in Figure 7 of Paper I. This is important as it shows that torsional waves can be generated directly in the corona and therefore the whole wave energy (i.e without any loses due to propagation from the photosphere and dynamic chromosphere to the corona, as is usually suggested can be dissipated in the corona. For example, regions with ($\beta < 1$) are perfect for the decay of torsional Alfvén waves into kinetic Alfvén waves, see e.g. cross-scale nonlinear coupling and plasma energization by Alfvén waves (Voitenko & Goossens 2005), excitation of kinetic Alfvén turbulence by MHD waves and energization of space plasmas (Voitenko & Goossens 2004) or the transformation of MHD Alfvén waves in space plasma (Fedun et al. 2004).

From a nearly vertical perspective of the jet, the vertical component of the velocity shows a blue-red shift, that is similar to the observed in the transition region and coronal lines as shown in Figure 18 of Martínez-Sykora et al. (2013), where the Doppler shifts correspond to velocities within the range -8 to 8 km s^{-1}. Finally, although there is no magnetoconvection, in the simulated plasma jet we conclude that rotational motion can still occur naturally at coronal heights without the need of any photospheric driver, e.g., granular buffeting or vortex motion. In fact, we have shown that such jets could be an in-situ driver of torsional Alfvén waves in the corona.
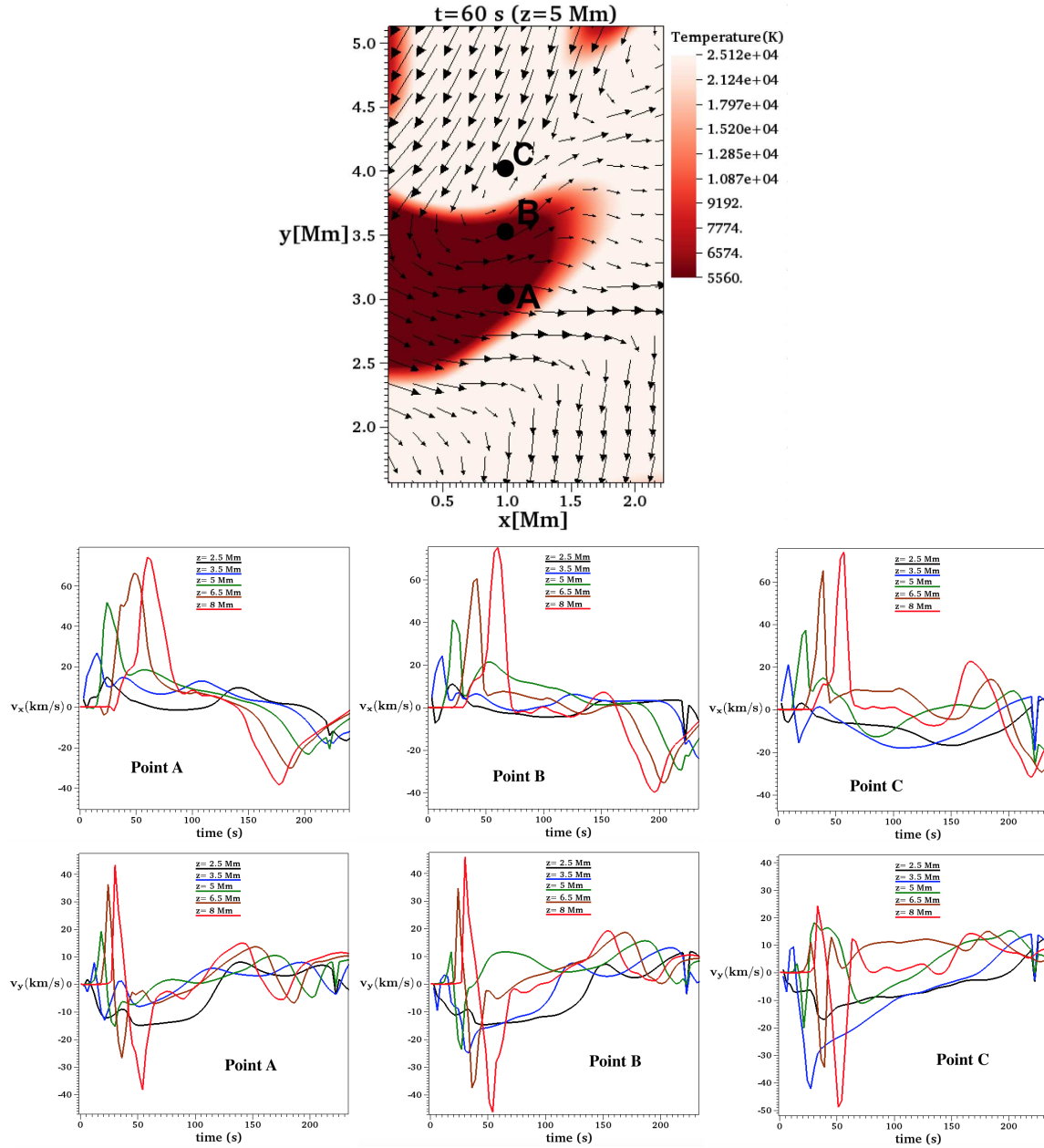
Figure 2.   In the top we show the region where v_x and v_y are measured. The color labels the temperature in the plane $z = 5$ Mm at time $t = 60$ s, where the structure of spicule and the circulation of the vector velocity field is clearly seen. In the middle and bottom panels we show the time series of v_x and v_y in km s^{-1} of the volume elements at the points A, B and C measured at various planes of constant height.

REFERENCES

Avrett, E. H., & Loeser, R. 2008, ApJS, 175, 229

Beckers, J. M. 1968, SoPh, 3, 367
Beckers, J. M. 1972, ARA&A, 10, 73
Cheung, M. C. M., De Pontieu, B., Tarbell, T. D., et al. 2015, ApJ, 801, 83
Curdt W., Heinzel P., Schmidt W., Tarbell T., Uexkull V., Wilken V. 1999, ed. A. Wilson (ESA SP-448;Noordwijk: ESA), 177
Curdt, W., & Tian, H. 2011, å, 532, L9
Curdt, W., Tian, H., & Kamio, S. 2012, SoPh, 280, 417
De Pontieu, B., Erdélyi, R., & James, S. P. 2004, Nature, 430 536
De Pontieu, B., McIntosh, S., Hansteen, V. H. 2007a, PASJ, 59, 655
De Pontieu, B., McIntosh, S., Carlsson, M. et al. 2007b, Science, 318, 1574
De Pontieu, B., McIntosh, S. W., Hansteen, V. H., & Schrijver, C. J. 2009, ApJ, 701, L1
De Pontieu, B., McIntosh, S. W., Carlsson, M., et al. 2011, Science, 331, 55
De Pontieu, B., Carlsson, M., Rouppe van der Voort, L. H. M., et al. 2012, ApJ, 752, L12
Dere, K. P., Bartoe, J.-D. F., & Brueckner, G. E. 1989, SoPh, 123, 41
Fedun, V. N., Yukhimuk, A. K., & Voitsekhovskaya, A. D. 2004, Journal of Plasma Physics, 70, 06
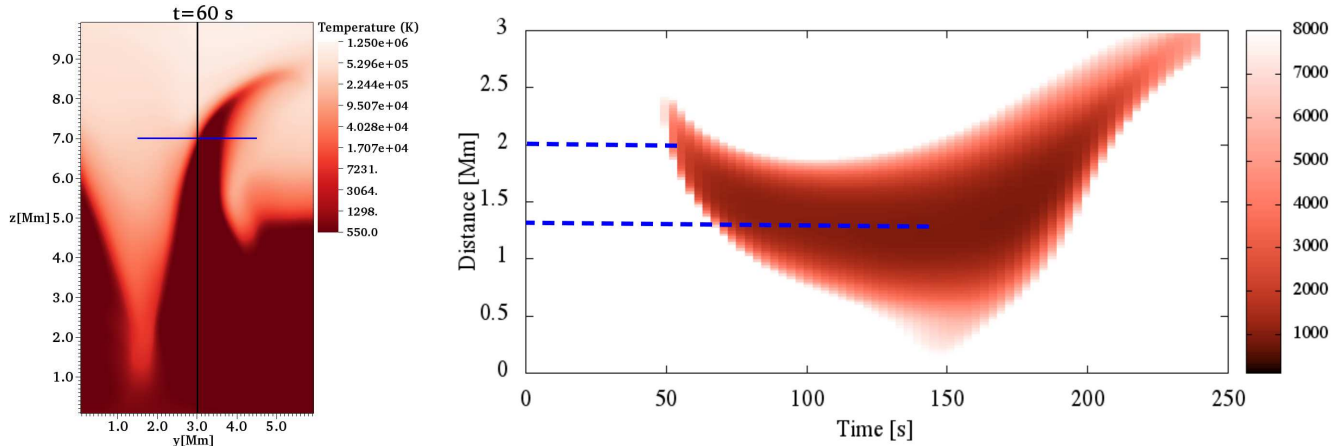Fontela, J. M., Avrett, E. H., & Loeser, R. 1990, ApJ, 355, 700

Figure 3. (Left) Snapshot of the logarithm of temperature (K) at time $t = 60$ s, vertical line in black at $y = 3$ Mm and horizontal line in blue from $y = 1.5$ Mm to $y = 4.5$ Mm at $z = 7$ Mm. (Right) The time-distance plot of logarithm of temperature (K) and dashed lines to estimate the average transverse speed.

González-Avilés, J. J., Guzmán, F. S., Fedun, V., Verth, G., Shelyag, S., & Regnier, S. 2018, ApJ, 856, 176

Griffiths, N. W., Fisher, G. H., Woods, D. T., & Siegmund, H. W. 1999, ApJ, 512, 992

Hansteen V. H., De Pontieu B., Ruoppe van der Voort L., van Noort M., Carlsson M. 2006, ApJ, 647, L73

He, J., Marsch, E., Tu, C., & Tian, H. 2009, ApJ, 705, L217

Jiang R. L., Fang C., Chen P. F. 2012, Comp. Phys. Comm., 183, 1617

Kayshap, P., Murawski, K., Srivastava, A. K., & Dwivedi, B. N. 2018, arXiv:1805.02517

Kuridze, D., Morton, R. J., Erdélyi, R., Dorrian, G. D., Mathioudakis, M., Jess, D. B., & Keenan, F. P. 2012, ApJ, 750, 51

Liu, W., Berger, T. E., Title, A. M., & Tarbell, T. D. 2009, ApJ, 707, L37

Liu, W., Berger, T. E., Title, A. M., Tarbell, T. D., & Low, B. C. 2011, ApJ, 728, 103

McIntosh, S. W., De Pontieu, B., Carlsson, M., et al. 2011, Nature, 475, 477

McLaughlin, J. A., Verth, G., Fedun, V., & Erdélyi, R. 2012, ApJ, 749, 30

Martínez-Sykora, J., Hansteen, V., & Carlsson, M. 2009, ApJ, 702, 129

Martínez-Sykora, J., Hansteen, V., & Moreno-Insertis, F. 2011, ApJ, 736, 9

Martínez-Sykora, J., De Pontieu, B., Leenaarts, J., et al. 2013, ApJ, 771, 66

Martínez-Sykora, J., De Pontieu, B., Hansteen, V. H., Roupe van der Voort, L., Carlsson, M., & Pereira, T. M. D. 2017, Science, 356, 1269

Matsumoto, T., & Shibata, K. 2010, ApJ, 710, 1857

Nishizuka, N., et al. 2008, ApJ, 683, L83

Okamoto, T. J., & De Pontieu, B. 2011, ApJ, 736, L24

Pariat, E., Dalmasse, K., DeVore, C. R., Antiochos, S. K., & Karpen, J. T. 2016, A&A, 596, A36

Pereira, T. M. D., De Pontieu, B., & Carlsson, M. 2012, ApJ, 759, 18

Pereira, T. M. D., De Pontieu, B., & Carlsson, M., et al. 2014, ApJ, 792, L15

Pike, C. D., & Mason, H. E. 1998, SoPh, 182, 333

Scullion, E., Erdélyi, R., Fedun, V., & Doyle, J. G. 2011, ApJ, 743, 14

Skogsrud, H., Roupe van Der Voort, L., & De Pontieu, B. 2014, ApJ, 795, L23

Skogsrud, H., Roupe van Der Voort, L., De Pontieu, B., & Pereira, T. M. D. 2015, ApJ, 806, 170

Secchi, A., Die Sterne: Grundzuge der Astronomie der Fixsterne (Brockhaus, 1878)

Sekse, D. H., Rouppe van der Voort, L., & De Pontieu, B. 2012, ApJ, 752, 108

Sekse, D. H., Rouppe van der Voort, L., De Pontieu, B., & Scullion, E. 2013, ApJ, 769, 44

Sharma, R., Verth, G., & Erdélyi, R. 2017, ApJ, 840, 96

Shibata, K., Nishikawa, T., Kitai, R., & Suematsu, Y. 1982, SoPh, 77,121

Shibata, K., Nakamura, T., & Matsumoto, T., et al. 2007, Science, 318, 5856

Shelyag, S., Mathioudakis, M., & Keenan, F. P. 2012, ApJ, 753, L22

Shetye, J., Doyle, J. G., & Scullion, E., et al. 2016, å, 589, A3

Srivastava, A. K., Shetye, J., & Murawski, K., et al. 2017, Sci. Rep. 7, 43147

Sterling, A. C. 2000, SoPh, 196, 79

Sterling, A. C., Harra, L. K., & Moore, R. 2010a, ApJ, 722, 1644

Sterling, A. C., Moore, R., & DeForest, C. E. 2010b, ApJ, 714, L1

Suematsu, Y., Wangm H., & Zirin, H. 1995,ApJ, 450, 411

Suematsu, Y., Ichimito, K., Katsukawa, Y., et al. 2008, in ASP Conf. Ser. 397, First Results From Hinode, ed. S. A. Matthews, J. M. Davis, & L. K. Harra (San Francisco, CA: ASP), 27

Tavabi, E., Koutchmy, S., & Golub, L. 2015, SoPh, 290, 2871

Tian, H., DeLuca, E., Cranmer, S. R., et al. 2014, Science, 346, 1255711

Tomczyk, S., McIntosh, S. W., Keil, S. L., Judge, P. G., Schad, T., Seeley, D. H., & Edmondson, J. 2007, Science, 317, 1192

Vögler, A., Shelyag, S., Schüssler, M., et al. 2005, A&A, 429, 335

Voitenko, Y., & Goossens, M. 2004, Nonlin. Processes Geophys., 11, 535

Voitenko, Y., & Goossens, M. 2005, Phys. Rev. Lett., 94, 135003

Zaqarashvili, T. V., & Erdélyi, R. 2009, Space. Sci. Rev., 149, 355

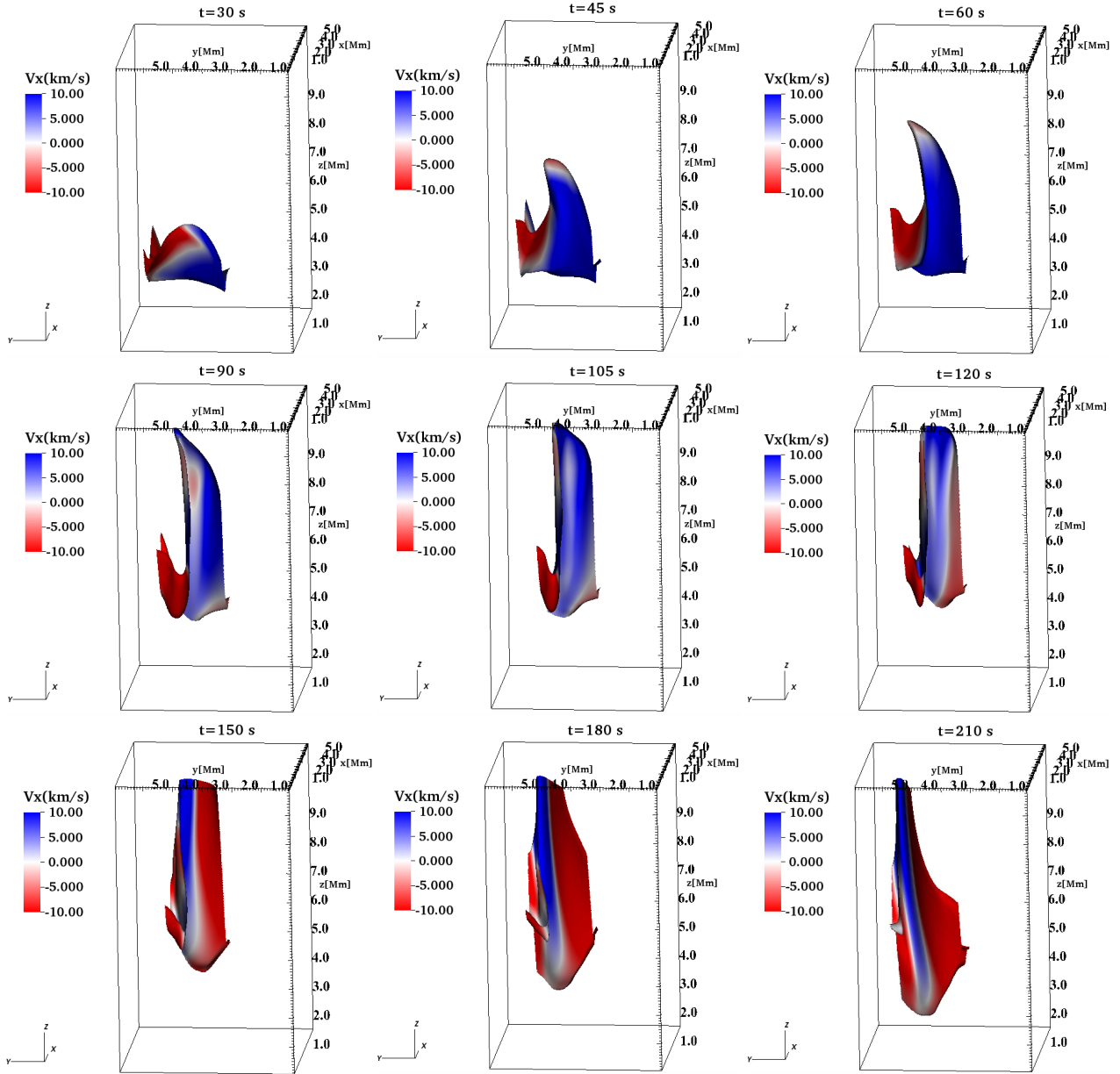Zhang, Y. Z., Shibata, K., Wang, J. X., et al. 2012, ApJ, 750, 16

Figure 4. Snapshots of a temperature contour at various times. The jet is represented by an isosurface of the plasma temperature equal to 10^4 K. The color-code labels the value of v_x. In this perspective blue indicates motion toward the reader and red toward inside the page.
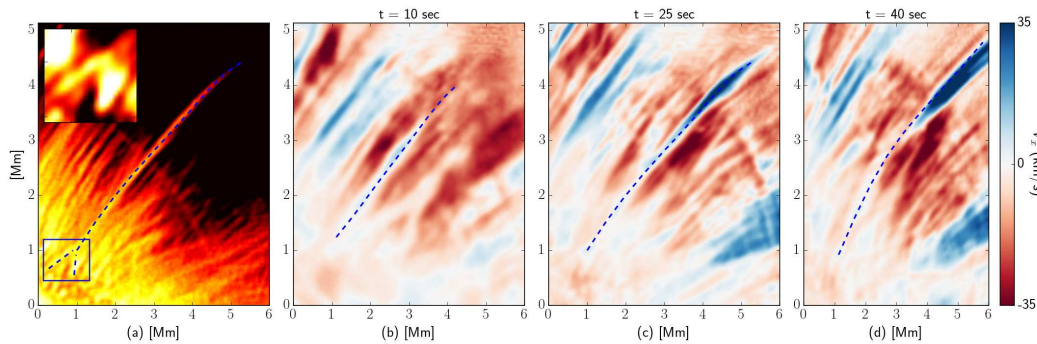

Figure 5. Left to right: Panels show a spicule (traced as dashed-line) off-limb, observed in Hα wavelength (a), with temporal evolution of the line-of-sight (LOS) Doppler velocity estimates (b-d). The unsharp-masked intensity image (a) show inverted Y-shaped structure (zoomed in inset) at the spicule footpoint (highlighted in box) suggestive of a magnetic reconnection process. Doppler estimates reveal the longitudinal rise of the spicule with its dominant motion towards the observer (b-c). The development of rotational motion is indicated by the enhanced red-blue asymmetric profile at the apex of spicule (d).
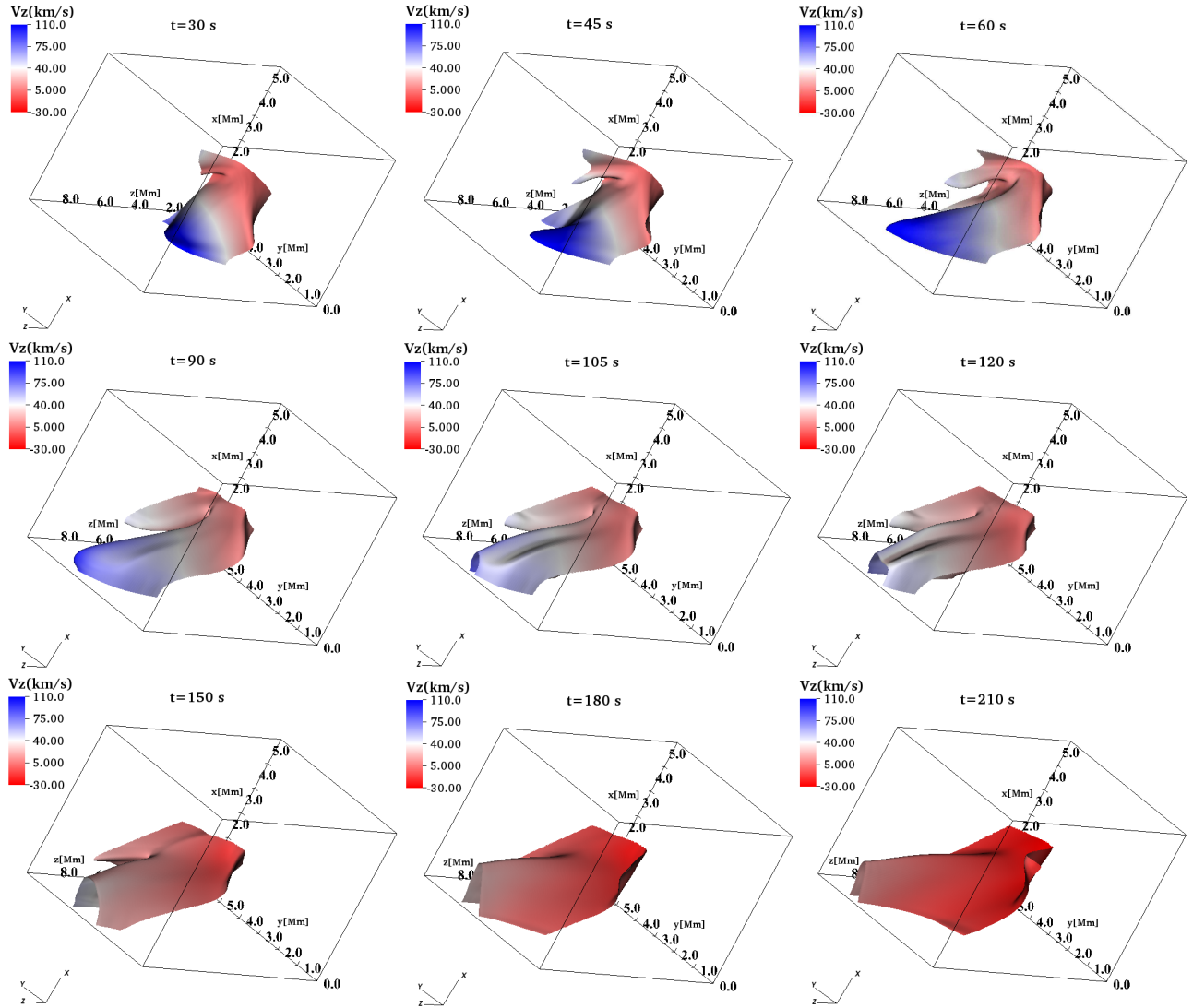
Figure 6. Snapshots of a temperature contour at various times. The jet is represented by an isosurface of the plasma temperature equal to 10^4 K. The color-code labels the value of v_z. The color red and blue indicates downward and upward velocity respectively.
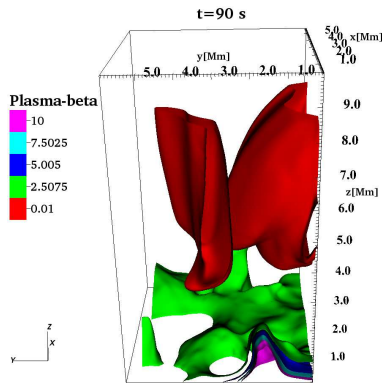

Figure 7. Contours of plasma β at time t=90 s. The contours indicate that magnetic field is dominant in the region where the spicule is formed as is shown in Figure 4.